Compressibility, Phase Transition, and Argon Insertion in the Siliceous Zeolite Mobil-Twelve at High Pressure

Damian Paliwoda, Marco Fabbiani, Frederico Alabarse, Patrick Hermet, Jérôme Rouquette, Francesco Di Renzo, Julien Haines

To cite this version:

Damian Paliwoda, Marco Fabbiani, Frederico Alabarse, Patrick Hermet, Jérôme Rouquette, et al.. Compressibility, Phase Transition, and Argon Insertion in the Siliceous Zeolite Mobil-Twelve at High Pressure. Journal of Physical Chemistry C, 2022, 126 (5), pp.2877-2884. 10.1021/acs.jpcc.1c10054. hal-03628394

HAL Id: hal-03628394
https://hal.umontpellier.fr/hal-03628394v1

Submitted on 30 May 2022

Compressibility, Phase Transition and Argon Insertion in the Siliceous Zeolite Mobil Twelve at High Pressure

Damian Paliwoda[†], *Marco Fabbiani*[†], *Frederico Alabarse*[‖], *Patrick Hermet*[†], *Jérôme Rouquette*[†], *Francesco Di Renzo*[†], *Julien Haines**[†]

[†]ICGM, CNRS, Université de Montpellier, 34293 Montpellier, France.

[‖]Elettra Sincrotrone Trieste, Trieste, 34149 Italy

*email: Julien.Haines@umontpellier.fr

ABSTRACT

The siliceous zeolite Zeolite Socony Mobil-twelve (ZSM-12) or MTW (Mobil-TWelve) with a 1-dimensional pore system was studied at high pressure by synchrotron x-ray powder diffraction in non-penetrating DAPHNE7474 oil and in a penetrating argon pressure medium. A phase transition from the space group $C2/c$ to $P2/n$ is observed in the non-penetrating medium at close to 1.5 GPa with a 4% volume decrease and a strong increase in compressibility in the *ac* plane corresponding to partial collapse of the pores. Strong decreases in diffracted intensity are observed with further compression and the diffraction pattern contains broad features characteristic of an amorphous material above 10 GPa. Distinct behavior is observed when this material is pressurized in argon. Argon fills the pores with 9±1 Ar atoms per unit cell. In this medium-pore zeolite, the quantity of inserted argon was not found to vary with pressure. Argon-filled MTW is 35% less compressible than the corresponding empty form.

1. Introduction

Zeolites are microporous materials with pore diameters of less than 1 nm, built up of rings and cages of corner-sharing TO_4 (T=Si, Al) tetrahedra. Due to their porosity, zeolites have a large number of applications in catalysis, as molecular sieves and sorbents, for example. A consequence of porosity is that such structures can potentially collapse under the influence of high pressure giving rise to phase transitions and pressure-induced amorphization (PIA). There are several examples (ANAlcime-ANA, zeolite-RHO-RHO, Linde Type A-LTA, Virgina Polytechnic Institute-FIve-VFI, Theta-ONe-TON) of high pressure phase transitions involving distortion and partial collapse of the pores of zeolites[1-5]. At higher pressures, PIA is widespread, giving rise to novel amorphous materials[4-12].

Guest insertion under pressure, in particular, in the case of noble gas elements in high silica zeolites, results in complete filling of the pores of the host zeolite. This can strongly modify the high pressure behavior of zeolites, by resisting the phenomenon of pore collapse and resulting phase transitions and PIA. Noble gases have been inserted in several small pore zeolites such as Mobil-FIve-MFI[13], NATrolite-NAT[14], LTA[15] and TON[16]. In TON, for example, the pores are filled gradually by Ne or Ar with pressure increase. The amount of Ar inserted is about a factor of 2 less than for Ne, and the kinetics of desorption are slow with argon remaining in the pores many hours after pressure release. In the case of Xe-filled LTA[17], the observed insertion is irreversible on pressure release. Another guest molecule of particular interest is water, which has been shown to give rise to energy storage properties in pure silica zeolites[18-20]. These zeolites can also be used as host materials for the polymerization of organic and inorganic molecules to form polymer/zeolite nanocomposites[21-26].

Zeolite Socony Mobil-twelve (ZSM-12) or Mobil TWelve (MTW) is high silica zeolite with a 1-D pore system[27]. The structure is monoclinic with a $C2/c$ space group[28]. MTW has slightly elliptical pores along the [010] direction based on 12-membered rings of SiO_4 tetrahedra. The elliptical pore diameter is 5.7 Å x 6.8 Å[29]. This system is of interest as a model, medium pore zeolite with empty 1-D pores due to the almost complete absence of charge compensating cations due to the high Si/Al ratio. This zeolite has been found to be particularly promising for energy storage upon water intrusion/extrusion at high pressure with a stored energy of 15 J/g for an intrusion pressure of 132 MPa[19].

The goal of the present study is to investigate the stability of the structure of this 1-D medium pore zeolite under high pressure by x-ray powder diffraction and also to study guest insertion of argon and its effect on the high pressure behavior of this material.

2. Experimental and theoretical methods

Microcrystalline MTW was prepared by sol-gel techniques using methyltriethylammonium chloride as the structure directing agent (SDA) with a molar composition of 0.2 Na : 0.2 SDA : 0.007 Al : Si : 20 H_2O. The crystallization was carried out at 140°C under hydrothermal conditions for 11 days and the obtained powder was calcined at 600°C for 5h. The Si:Al ratio of the crystals was found to be 41.9 by EDS analysis. The remaining sodium was exchanged using ammonium chloride, followed by a second calcination to obtain the protonic form of the zeolite. The nitrogen adsorption analysis at 77K showed a classical type I isotherm with an exposed specific surface area of 316 m^2/g and the total pore volume of 0.14 cm^3/g that corresponds to 100% of the total available porosity. The amount of adsorbed N_2 in the micropores was close to 2.9 mmol/g for the sodium form after the first calcination and close to 3.4 mmol/g for the protonic form after the second calcination.

High pressure synchrotron powder X-ray diffraction (λ=0.4957 Å) measurements in membrane-driven diamond anvil cells were performed with an 80 μm beam spot on the sample on the Xpress beamline equipped with a PILATUS3 S 6M (DECTRIS) detector at the ELETTRA Sincrotrone Trieste (Trieste, Italy). The XRD images (see supporting information) were converted to 1-D diffraction profiles using Dioptas[30] based on a calibration using NIST SRM 674b CeO_2 (a = 5.411651 Å[30]) as a standard. The sample to detector distance was determined to be 634.38 mm based on this calibration. The hole in the preindented stainless steel gasket was loaded with the submicronic MTW powder under an argon atmosphere in a glove box to avoid the presence of any H_2O molecules in the pores. A ruby microsphere was added as pressure calibrant. Pressure was measured before and after every x-ray exposure based on the shift of the ruby R_1 fluorescence line[31]. The standard deviations of the reported pressures are based on the values obtained before and after each exposure. In the first experiment, non-penetrating liquid DAPHNE7474[32] oil was used as the pressure-transmitting medium. In a second independent experiment, argon was loaded cryogenically in the liquid phase. Le Bail fits to obtain the unit cell parameters and Rietveld refinements were performed using the program Fullprof[33]. The quoted estimated standard deviations for the lattice parameters and the fractional atomic coordinates are those obtained directly from these refinements. Fractional atomic coordinates for the framework from previous work were used as the starting model for MTW[28]. Soft constraints were applied to the Si-O and O-O distances. An overall isotropic atomic displacement parameter (ADP) was used for all Si, O and Ar atoms as no improvement was obtained using individual ADPs. Crystal structures were plotted using the program VESTA[34]. EosFit[35] was used to fit the P-V data.

Structure relaxation (atomic positions and lattice parameters) was performed within the density functional theory as implemented in the SIESTA package[36]. No constraint was imposed during the relaxation. The structure was considered as relaxed when the maximum residual atomic force and the pressure are smaller than 0.03 eV/Å and $2\text{x}10^{-5}$ eV/Å^3, respectively. We used the generalized gradient approximation (GGA) to the exchange correlation functional as proposed by Perdew, Burke and Ernzerhof[37]. Core electrons are replaced by nonlocal norm-conserving pseudopotentials. The valence electrons are described by a double-zetaζ singly polarized basis set. The localization of the basis is controlled by an energy shift of 50 meV. Real space integration is performed on a regular grid corresponding to a plane-wave cutoff of 350 Ry and using a 3x9x3 k-points mesh. Van der Waals corrections (DFT-D3) are included in our calculations using the semi-empirical dispersion potential parametrized by Grimme[38].

Results and discussion

MTW powder was first studied in the nonpenetrating DAPHNE7474 pressure transmitting medium to determine the intrinsic high-pressure behavior of this framework (Figure 1). The structure of MTW in the diamond anvil cell at close to ambient pressure was refined by the Rietveld method based on the structural model of MTW with a *C*2/*c* space group from the literature[28]. The initial unit cell parameters are: *a*=24.935(2) Å, *b*=5.0162(3) Å, *c*=24.349(1) Å, β=107.854(6)° (Table 1).

Based on Fourier difference maps, some electron density was identified in the pores, which may arise from residue of the SDA or from trace argon atoms in the pores as the MTW was stored and manipulated in a glove box under an argon atmosphere. This electron density was modelled using nitrogen atoms with partial occupancy placed on the maxima of electron density. The partial occupancies correspond to close to 3 N atoms or 1 Ar atom per unit cell. This structural model was used for the data up to a pressure of 1.53 GPa. Very good fits were obtained (Figures 2 and 3) and with excellent agreement factors ($R_{profile}$=12.7%, R_{Bragg}=8.4%). The principal changes are in the pore dimensions (Figures 4 and 5), which decrease from 5.6 Å x 6.9 Å at ambient pressure to 5.0 Å x 6.7 Å at 1.53 GPa. The pores thus become more elliptical (Figure 5). This is linked to much greater decreases in the intertetrahedral Si-O-Si bridging angles in and linked to the four-membered rings of tetrahedra along the pore walls, that is involving Si1 and Si2. In particular, the Si1-O2-Si2 angle decreases by 11.5(9)° between 0.25 and 1.53 GPa (Table 2). This is consistent with the compressibility along *c* being slightly higher than along *a* (Table 1 and Figure 6). The highest compressibility is observed along *b*, corresponding to an accordion-like deformation of the zigzag chains parallel to the pore axis.

Table 1. Unit cell parameters of the monoclinic *C*2/*c* and *P*2/*n* (in italics) phases of MTW in DAPHNE7474 and Ar as a function of pressure.

P(GPa)	*a*(Å)	*b*(Å)	*c*(Å)	*β*(°)	*V*(Å^3)
DAPHNE7474					
0.0001	24.935(2)	5.0162(3)	24.349(1)	107.854(6)	2898.9(3)
0.25(1)	24.822(1)	4.9865(2)	24.236(1)	107.772(6)	2856.8(3)
0.56(1)	24.674(2)	4.9481(3)	24.091(1)	107.704(6)	2801.9(3)
0.81(1)	24.582(2)	4.92462(3)	23.995(1)	107.659(7)	2767. 9(3)
1.53(2)	24.273(2)	4.8563(5)	23.660 (2)	107.48(1)	2660.2(4)
2.00(1)	*23.595(4)*	*4.850(1)*	*22.840(1)*	*107.06(2)*	*2498.5(9)*

2.16(5)	*23.537(5)*	*4.834(1)*	*22.868(5)*	*107.05(2)*	*2487(1)*
2.50(1)	*23.331(5)*	*4.826(1)*	*22.551(5)*	*106.83(3)*	*2430(1)*
2.54(3)	*23.282(5)*	*4.828(1)*	*22.475(5)*	*106.66(3)*	*2421(1)*
3.04(6)	*23.071(7)*	*4.811(2)*	*22.256(7)*	*106.49(3)*	*2368(1)*
3.61(4)	*22.77(2)*	*4.791(3)*	*21.943(9)*	*106.04(6)*	*2300(2)*
Ar					
0.29(1)	24.914(2)	5.0050(3)	24.345(1)	107.90(1)	2888.7(4)
0.52(1)	24.858(3)	4.987(5)	24.295(2)	107.89(1)	2866.1(5)
0.83(1)	24.774(4)	4.9574(6)	24.218(3)	107.88(1)	2830.6(6)
1.19(1)	24.686(4)	4.9338(7)	24.136(3)	107.85(2)	2798.2(7)
1.52(2)	24.577(5)	4.9015(8)	24.038(4)	107.82(2)	2756.7(8)
1.80(3)	24.531(6)	4.887(1)	23.994(4)	107.81(2)	2738(1)

Above 1.53 GPa, a series of new reflections, such as $\bar{1}01$, 101, $\bar{3}01$, $\bar{1}03$ and 301 for example, are observed in the diffraction pattern of MTW. These reflections violate the reflection conditions of the *C*2/*c*, space group, and imply the loss of *C*-centering, and the *c* glide planes. The reflections are consistent with a primitive monoclinic cell with slightly decreased *a* and *c* lattice parameters (Figure 6) and a volume change at 2 GPa of around 4% (Figure 7). The *b* parameter is relatively unaffected. The monoclinic angle also decreases confirming that the changes occur principally in the *ac* plane, which also becomes more compressible.

The possible monoclinic subgroups of the *C*2/*c* space group, taking into loss of the *C*-centering and the *c* glide plane are *P*2/*n*, $P2_1/n$, *P*2 and $P2_1$. Possible shoulders could correspond to 203 and 300 reflections indicating that the *n* glide might also be lost. Some of the low pressure *C*2/*c* phase remained untransformed amounting to close to 10% at 2.16 GPa and 8% at hydrostatic limit of the DAPHNE7474 fluid near 4 GPa. The high pressure phase is clearly a low symmetry distortion of the starting *C*2/*c* phase, based on the large number of common reflections with similar intensities. Attempts were thus made to refine the structure of the new phase in the highest symmetry monoclinic subgroup $P2/n$ starting with atomic positions of the low pressure phase. During the refinement cycles the agreement factors improved rapidly leading to a structural model with collapsed pores. In order to have a less arbitrary configuration, the resulting model was relaxed by DFT. The resulting structure yielded very good agreement with the experimental data with a Bragg R-factor of 8.7% using the experimental lattice parameters. Similar agreement factors were obtained using this relaxed structure as a starting model in Rietveld refinements. The experimental lattice parameters, a=23.537(5) Å, b=4.834(1) Å, c=22.868(5) Å, β=107.05(2)° are compared to the relaxed values a=23.8995 Å, b=4.8929 Å, c= 23.5694 Å, β= 106.727°. This slight overestimate is commonly observed at the GGA level. Attempts using the $P2_1/n$ and $P2_1$ space groups resulted in strong distortion to the framework and poor agreement values. It is possible that the structure is in fact $P2$ with a many more degrees of freedom, but the present two-phase data cannot clearly be used to support such a distortion with three different types of pores. In addition, the DFT calculations were performed with no symmetry constraints and converged readily to give $P2/n$ symmetry.

Table 2. Intertetrahedral Si-O-Si bridging angles (°) along the pore walls as function of pressure. Angles lying principally out of the *ac* plane are in italics. Atom labels correspond to the CIF files in SI.

	DAPHNE7474			Argon		
	0.25 GPa	1.53 GPa	difference	0.29 GPa	1.52 GPa	difference
Si1-O2-Si2	152.1(5)	140.6(5)	-11.5(9)	154.2(5)	148.9(5)	-5.3(10)
Si3-O3-Si1	*143.3(5)*	*136.8(5)*	*-6.5(10)*	*143.6(5)*	*139.5(5)*	*-4.1(10)*
Si3-O12-Si1	*143.3(5)*	*135.5(5)*	*-7.8(10)*	*143.6(5)*	*136.5(5)*	*-7.1(10)*
Si7-O6-Si3	140.0(4)	134.2(5)	-5.8(9)	140.8(4)	136.3(4)	-4.5(8)
Si7-O11-Si6	155.3(5)	151.2(6)	-4.1(11)	155.3(5)	152.8(6)	-2.5(11)
Si4-O9-Si6	136.1(6)	131.1(6)	-5.0(12)	138.6(6)	136.4(6)	-2.2(12)
Si4-O13-Si2	*145.1(5)*	*137.3(6)*	*-7.8(11)*	*146.3(5)*	*139.5(5)*	*-6.9(10)*
Si2-O5-Si4	*151.3(5)*	*142.6(6)*	*-8.7(11)*	*153.4(5)*	*147.3(5)*	*-6.1(10)*

The P-V data were fitted to a second-order Birch-Murnaghan equation of state[39]. The fit for the low-pressure *C*2/*c* phase yielded a bulk modulus B_0 of 15.5(2) GPa, which is typical of empty siliceous zeolites, such as MFI[11-12] and TON[5] and other empty porous materials, such as metal-organic frameworks[40-42]. The corresponding value for the *P*2/*n* phase is 9.4(4) GPa with an initial relative volume of 1.007(6). If the initial relative volume is fixed to 1, a B_0 of 9.95(4) GPa is obtained, but the fit is poorer. The higher compressibility of the *P*2/*n* phase is due to its high flexibility arising from its lower symmetry, which allows for additional compression mechanisms and more flexibility of the zeolitic framework. This additional flexibility in the lower symmetry phase allows for progressive pore collapse as a function of pressure. Similar behavior with increased compressibility in high pressure, low symmetry phases due to additional compression mechanisms has been observed in zeotypes, such as ANA[1], including the minerals wairakite[43] and leucite[44], and TON[5], and also in other framework solids, such as zinc cyanide[45]. The pore diameters are 4.97Å x 6.70 Å at 1.53 GPa in the *C*2/*c* phase and 3.54 Å x 9.30 Å and 3.83 Å x 8.23 Å at 2.16 GPa in the *P*2/*n* phase. This mechanism is similar to that reported for TON[5]. This transition was found to be reversible with some degree of hysteresis and trace amounts of the *P*2/*n* phase persists even at 0.5 GPa. Further compression of the *P*2/*n* phase resulted in a gradual broadening of the diffraction lines and at pressures above 10 GPa, only broad features remain characteristic of an amorphous form as has been found for many other zeolites at high pressure[4-7, 9-12].

Distinct behavior is observed when MTW is compressed in argon up to 1.8 GPa, the pressure at which Ar was observed to be solid. All other points correspond to Ar in the liquid phase. At low pressures, the unit cell parameters and volume are significantly greater due to argon filling (Figures 6 and 7) and many, intertetrahedral Si-O-Si angles increase in particular the angles principally in the *ac* plane along the pore walls (Table 2). In addition, the diffraction lines become broader and less symmetrical with increasing pressure. Similar broadening due to guest insertion has been observed in TON and can be related to strain induced by the filling process[16]. In the non-penetrating DAPHNE7474, the diffraction lines remain sharp and symmetrical in the same pressure range.

In order to determine the structure of Ar-filled MTW, the MTW structure in the non-penetrating pressure medium was used as a starting model and Fourier difference maps were used to locate the Ar atoms. Refinements (Figure 2) were performed with the Ar atoms partially occupying 3-5 sites in a disordered arrangement (Figure 3, CIF file in Supporting Information). The argon content was found to be 9(1) Ar/atoms per unit cell and was found to be independent of pressure over the range from 0.29 to 1.52 GPa and is slightly lower than the value obtained for nitrogen in adsorption isotherms, which is close to 11 N_2 molecules per unit cell at 77 K. This indicates that in this medium-pore zeolite, complete filling readily occurs at very low pressure, in contrast to small-pore zeolites such as TON[16], which has 4.6 Å x5.6 Å diameter pores, for which filling is gradual over this pressure range. Pressure thus is less critical for optimal pore filling of argon in this medium-pore zeolite. In MTW and TON, there are essentially the same number of Ar atoms per pore just below the solidification of Ar near 1.5 GPa[46]. Initially, in the larger MTW pores at low pressure, there is more available space for the number of argon atoms inserted. In the case of argon filling in MTW, the short pore diameter increases strongly with respect to MTW at ambient pressure (Figure 5) and is close to 50% less compressible than when the pores are empty. This indicates that the structure has a degree of flexibility to accommodate the argon atoms. Another difference with respect to TON is that the pore ellipticity only increases slightly in Ar-filled MTW under pressure, whereas a very strong increase in ellipticity is observed in Ar-filled TON[16] in a similar manner to empty TON[5]. Above 0.6 GPa, TON already adopts a high pressure structure with collapsed pores. Pressure is a factor in ensuring the filling with argon of these pores in TON, which are progressively collapsing. The short pore diameter in MTW lies along **c**, which becomes the most incompressible direction in the filled system (Figure 6). This can be correlated with the much smaller decrease in the intertetrahedral Si1-O2-Si2 bridging angle in the four-membered rings of tetrahedra along the pore walls (Table 2). The presence of Ar in the pores greatly reduces the compression (a,c) and distortion (β) in the ac plane, which correspond to the most affected parameters prior to and at the phase transition in empty MTW. The overall compressibility of Ar-filled MTW is 35% lower than that of empty MTW. The bulk modulus is 23.8(6)

GPa with an initial relative volume of 1.009(1). Upon decompression from 1.8 GPa down to 0.27 GPa, the observed behavior is reversible in terms of unit cell volume, but the diffraction lines remain strongly broadened and asymmetrical.

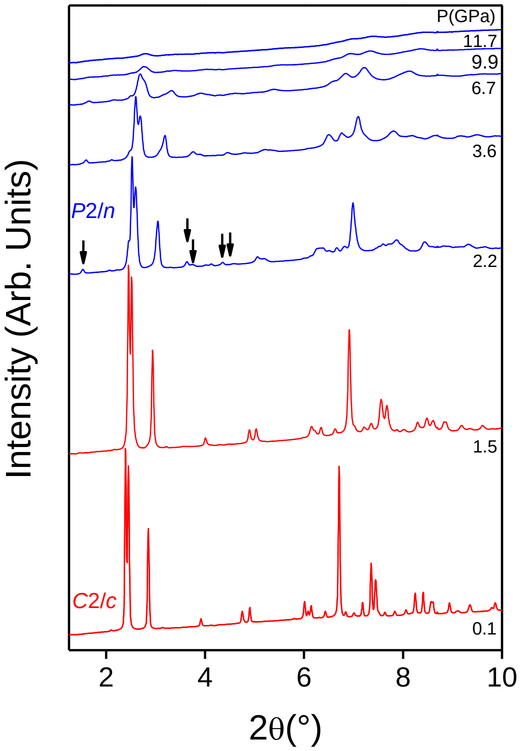

Figure 1. X-ray diffraction profiles of MTW in non-penetrating DAPHNE7474 oil (λ=0.4957 Å). Arrows indicate the principal additional reflections of the *P*2/*n* phase.

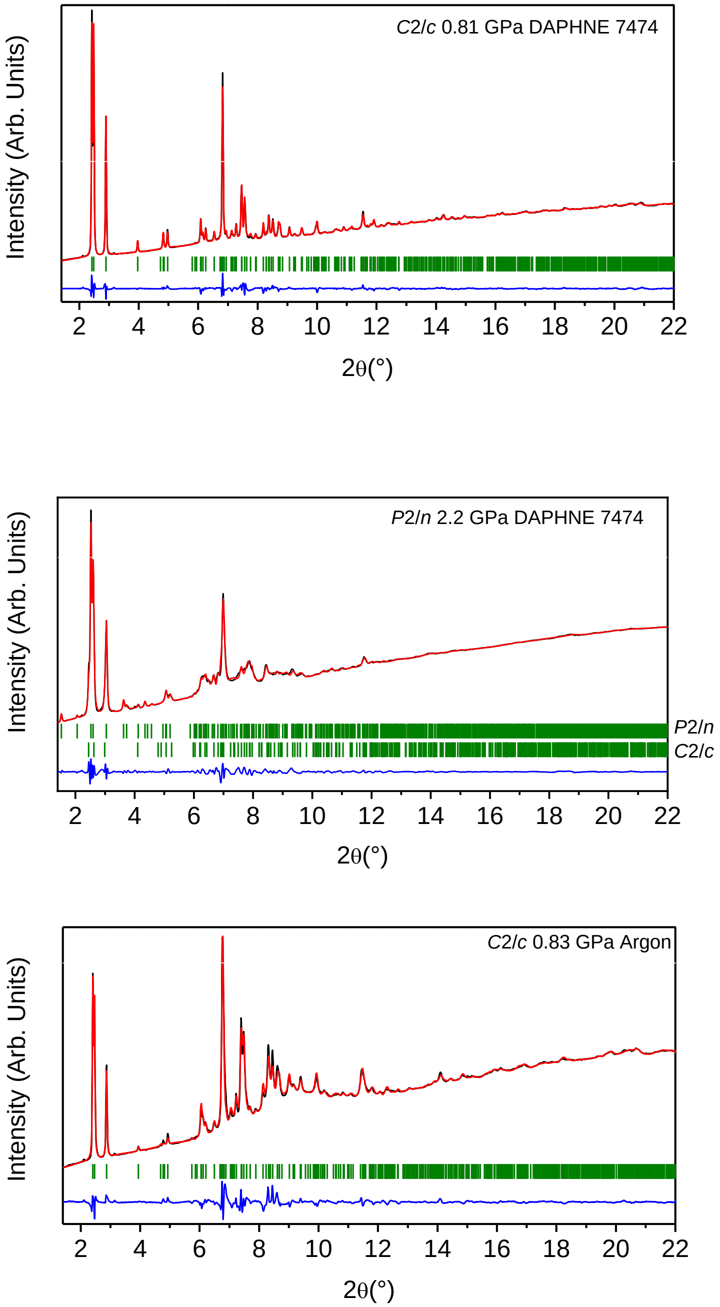

Figure 2. Experimental (black), calculated (red) and difference (blue) profiles (λ=0.4957 Å) for the Rietveld refinements of the *C*2/*c* structure of MTW at 0.81 GPa (above), the *P*2/*n* structure of MTW at 2.16 GPa in DAPHNE7474 (center) and the *C*2/*c* structure of MTW in argon at 0.83 GPa (below). Vertical bars indicate the calculated positions of the Bragg reflections. The pattern at 2.16 GPa corresponds to 90% *P*2/*n* and 10% remaining *C*2/*c* phases.

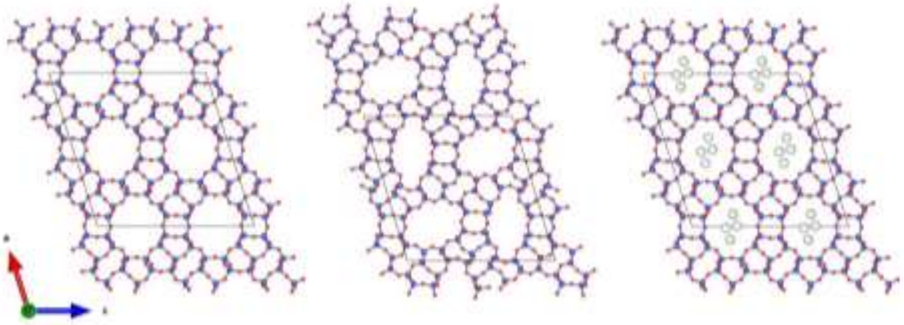

Figure 3. Refined crystal structure of *C*2/*c* structure of MTW at 0.81 GPa in DAPHNE7474 (left) and the relaxed *P*2/*n* structure of MTW at 2.16 GPa (middle) and the refined *C*2/*c* structure of MTW in argon at 0.83 GPa (right). In the crystal structures, the blue and red spheres represent the silicon and oxygen atoms, respectively. Argon atoms are represented by large empty spheres.

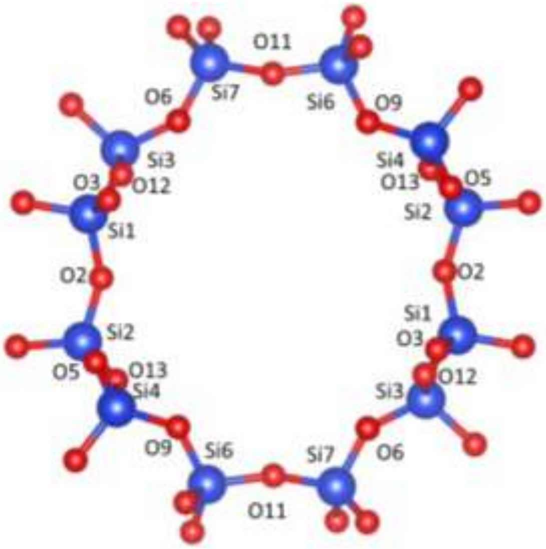

Figure 4. Detail of the refined crystal structure of *C*2/*c* phase of MTW at 0.25 GPa in DAPHNE7474 with the labels of the Si and O atoms in the pore walls. The blue and red spheres represent the silicon and oxygen atoms, respectively.

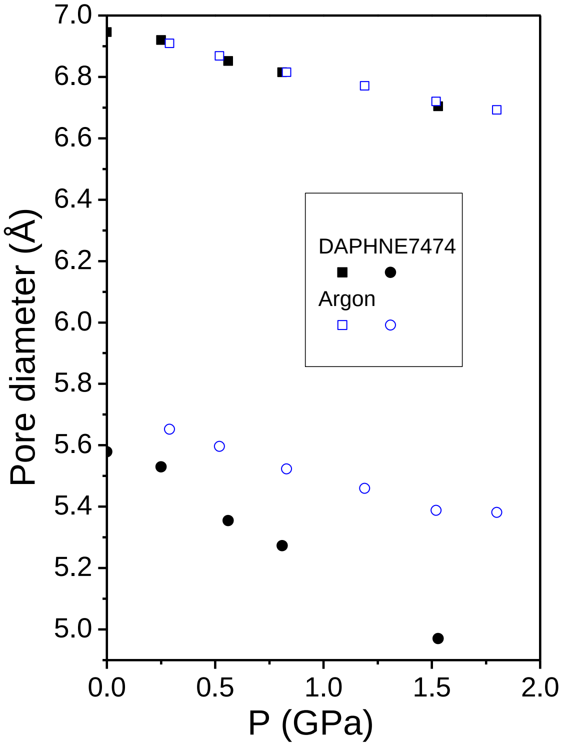

Figure 5. Minimum and maximum pore diameters of MTW in DAPHNE7474 (black symbols) and in argon (empty blue symbols).

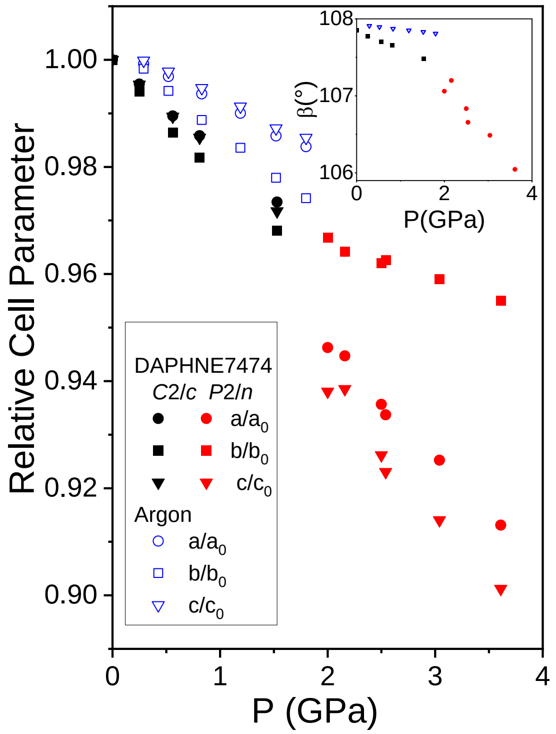

Figure 6. Relative cell parameters of MTW in DAPHNE7474 (black and red symbols) and in argon (empty blue symbols).

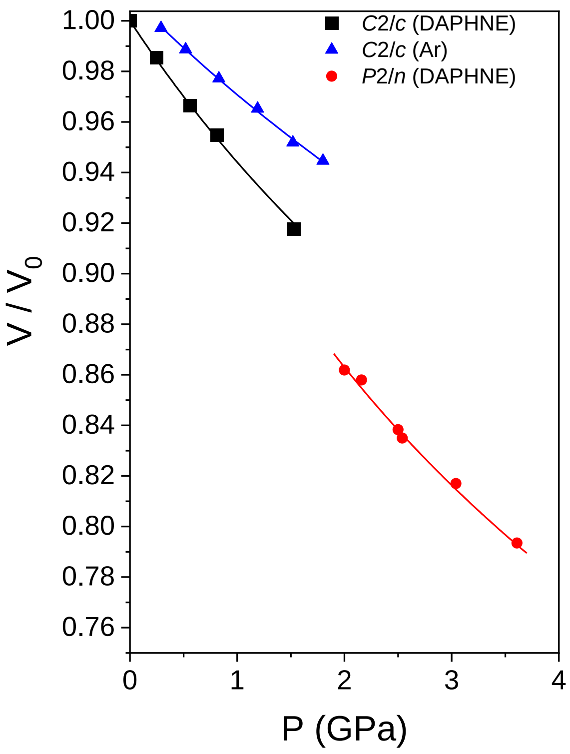

Figure 7. Relative volume (V/V_0) of MTW in DAPHNE7474 (black and red symbols) and in argon (blue symbols). Continuous lines represent equations of state with the B_0 and V_0 values given in the text.

3. Conclusions

The siliceous medium-pore zeolite MTW exhibits an increase in the ellipticity of its pores with compression. At close to 1.5 GPa, a phase transition from the *C*2/*c* to the *P*2/*n* structure is observed with a 4% volume change due to pore collapse. Further compression leads to gradual amorphization. Argon readily fills the pores of MTW with a constant value of 9(1) Ar atoms/unit cell over the pressure range investigated. This contrasts with the gradual filling observed for the small-pore zeolite TON. The short pore diameter is close to 50% less compressible due to argon filling and this is the principle origin of the 35% lower compressibility of the structure when compressed in argon. The present results on phase stability and pore filling of MTW at high pressure will be of great value for designing and synthesizing nanocomposite materials based on MTW and also for the use of MTW in energy storage applications.

ASSOCIATED CONTENT

Supporting Information. Selected 2-D powder x-ray diffraction patterns (PDF file) and crystallographic information files (CIF) files containing the structural data for the MTW-DAPHNE7474 at 0.25, 0.81 and 1.53 GPa, the MTW-Ar at 0.29, 0.83 and 1.52 GPa and the relaxed crystal structure of $P2_1/n$ MTW at 2.2GPa have been supplied as supporting information. This material is available free of charge via the Internet at http://pubs.acs.org.

AUTHOR INFORMATION

Corresponding Author

*Julien Haines

Julien.Haines@umontpellier.fr

Author Contributions

The manuscript was written through contributions of all authors. All authors have given approval to the final version of the manuscript.

Notes

The authors declare no competing financial interests.

ACKNOWLEDGMENT

We acknowledge funding from the Agence Nationale de la Recherche in the framework of the contracts ANR-19-CE08-0016 and ANR-19-CE09-0019. The research leading to this result has been supported by the project CALIPSOplus under Grant Agreement 730872 from the EU Framework Programme for Research and Innovation HORIZON 2020. The synchrotron X-ray diffraction experiments were performed at the Xpress beamline from Elettra Sincrotrone Trieste (proposal number: 20205124).

REFERENCES

1. Gatta, G. D.; Nestola, F.; Ballaran, T. B., Elastic Behavior, Phase Transition, and Pressure Induced Structural Evolution of Analcime. *Am. Mineral.* **2006**, *91*, 568-578.

2. Lee, Y.; Hriljac, J. A.; Vogt, T.; Parise, J. B.; Edmondson, M. J.; Anderson, P. A.; Corbin, D. R.; Nagai, T., Phase Transition of Zeolite Rho at High-Pressure. *J. Am. Chem. Soc.* **2001**, *123*, 8418-8419.

3. Jorda, J. L.; Rey, F.; Sastre, G.; Valencia, S.;;Palomino, M.; Corma, A.; Segura, A.; Errandonea, D.; Lacomba, R.; Manjon, F. J. et al., Synthesis of a Novel Zeolite through a Pressure-Induced Reconstructive Phase Transition Process. *Angew. Chem. Int. Edit.* **2013**, *52*, 10458-10462.

4. Alabarse, F. G.; Brubach, J. B.; Roy, P.; Haidoux, A.; Levelut, C.; Bantignies, J. L.; Cambon, O.; Haines, J., AlPO$_4$-54-AlPO$_4$-8 Structural Phase Transition and Amorphization under High Pressure. *J. Phys. Chem. C* **2015**, *119*, 7771-7779.

5. Thibaud, J. M.; Rouquette, J.; Hermet, P.; Dziubek, K.; Gorelli, F. A.; Santoro, M.; Garbarino, G.; Alabarse, F. G.; Cambon, O.; Di Renzo, F. et al., High-Pressure Phase Transition, Pore Collapse, and Amorphization in the Siliceous 1D Zeolite, TON. *J. Phys. Chem. C* **2017**, *121*, 4283-4292.

6. Greaves, G. N.; Meneau, F.; Sapelkin, A.; Colyer, L. M.; Gwynn, I. A.; Wade, S.; Sankar, G., The rheology of collapsing zeolites amorphized by temperature and pressure. *Nat. Mater.* **2003**, *2*, 622-629.

7. Greaves, G. N.; Meneau, F.; Kargl, F.; Ward, D.; Holliman, P.; Albergamo, F., Zeolite Collapse and Polyamorphism. *J. Phys.-Condens. Mat.* **2007**, *19*, 415102.

8. Huang, Y. M., IR Spectroscopic Study of the Effects of High Pressure on Zeolites Y, a and Sodalite. *J. Mater. Chem.* **1998**, *8*, 1067-1071.

9. Isambert, A.; Angot, E.; Hebert, P.; Haines, J.; Levelut, C.; Le Parc, R.; Ohishi, Y.; Kohara, S.; Keen, D. A., Amorphization of Faujasite at High Pressure: An X-Ray Diffraction and Raman Spectroscopy Study. *J. Mater. Chem.* **2008**, *18*, 5746-5752.

10. Readman, J. E.; Forster, P. M.; Chapman, K. W.; Chupas, P. J.; Parise, J. B.; Hriljac, J. A., Pair Distribution Function Analysis of Pressure Treated Zeolite Na-A. *Chem. Commun.* **2009**, 3383-3385.

11. Haines, J.; Levelut, C.; Isambert, A.; Hebert, P.; Kohara, S.; Keen, D. A.; Hammouda, T.; Andrault, D., Topologically Ordered Amorphous Silica Obtained from the Collapsed Siliceous Zeolite, Silicalite-1-F: A Step toward "Perfect" Glasses. *J. Am. Chem. Soc.* **2009**, *131*, 12333-12338.

12. Vezzalini, G.; Arletti, R.; Quartieri, S., High-Pressure-Induced Structural Changes, Amorphization and Molecule Penetration in MFI Microporous Materials: A Review. *Acta Crystallogr. B* **2014**, *70*, 444-451.

13. Haines, J.; Cambon, O.; Levelut, C.; Santoro, M.; Gorelli, F.; Garbarino, G., Deactivation of Pressure-Induced Amorphization in Silicalite SiO$_2$ by Insertion of Guest Species. *J. Am. Chem. Soc.* **2010**, *132*, 8860-8861.

14. Lee, Y.; Hriljac, J. A.; Vogt, T., Pressure-Induced Argon Insertion into an Auxetic Small Pore Zeolite. *J. Phys. Chem. C* **2010**, *114*, 6922-6927.

15. Niwa, K.; Tanaka, T.; Hasegawa, M.; Okada, T.; Yagi, T.; Kikegawa, T., Pressure-Induced Noble Gas Insertion into Linde-Type A Zeolite and Its Incompressible Behaviors at High Pressure. *Micropor. Mesopor. Mat.* **2013**, *182*, 191-197.

16. Thibaud, J. M.; Rouquette, J.; Dziubek, K.; Gorelli, F. A.; Santoro, M.; Garbarino, G.; Clement, S.; Cambon, O.; van der Lee, A.; Di Renzo, F. et al., Saturation, of the Siliceous Zeolite TON with Neon at High Pressure. *J. Phys. Chem. C* **2018**, *122*, 8455-8460.

17. Seoung, D.; Lee, Y.; Cynn, H.; Park, C.; Choi, K. Y.; Blom, D. A.; Evans, W. J.; Kao, C. C.; Vogt, T.; Lee, Y., Irreversible Xenon Insertion into a Small-Pore Zeolite at Moderate Pressures and Temperatures. *Nat. Chem.* **2014**, *6*, 835-839.

18. Eroshenko, V.; Regis, R. C.; Soulard, M.; Patarin, J., Energetics: A New Field of Applications for Hydrophobic Zeolites. *J. Am. Chem. Soc.* **2001**, *123*, 8129-8130.

19. Tzanis, L.; Trzpit, M.; Soulard, M.; Patarin, J., High Pressure Water Intrusion Investigation of Pure Silica 1D Channel AFI, MTW and TON-Type Zeolites. *Micropor. Mesopor. Mat.* **2011**, *146*, 119-126.

20. Tzanis, L.; Trzpit, M.; Soulard, M.; Patarin, J., Energetic Performances of Channel and Cage-Type Zeosils. *J. Phys. Chem. C* **2012**, *116*, 20389-20395.

21. Santoro, M.; Gorelli, F. A.; Bini, R.; Haines, J.; van der Lee, A., High-Pressure Synthesis of a Polyethylene/Zeolite Nano-Composite Material. *Nat. Commun.* **2013**, *4*, 1557.

22. Scelta, D.; Ceppatelli, M.; Santoro, M.; Bini, R.; Gorelli, F. A.; Perucchi, A.; Mezouar, M.; van der Lee, A.; Haines, J., High Pressure Polymerization in a Confined Space: Conjugated Chain/Zeolite Nanocomposites. *Chem. Mater.* **2014**, *26*, 2249-2255.

23. Santoro, M.; Dziubek, K.; Scelta, D.; Ceppatelli, M.; Gorelli, F. A.; Bini, R.; Thibaud, J. M.; Di Renzo, F.; Cambon, O.; Rouquette, J., et al., High Pressure Synthesis of All-Transoid Polycarbonyl [-(C=O)-]$_n$ in a Zeolite. *Chem. Mater.* **2015**, *27*, 6486-6489.

24. Santoro, M. Scelta, D.; Dziubek, K.; Ceppatelli, M.; Gorelli, F. A.; Bini, R.; Garbarino, G.; Thibaud, J.-M.; Di Renzo, F.; Cambon, O., et al., Synthesis of 1D Polymer/Zeolite Nanocomposites under High Pressure. *Chem. Mater.* **2016**, *28*, 4065-4071.

25. Paliwoda, D.; Comboni, D.; Poreba, T.; Hanfland, M.; Alabarse, F.; Maurin, D.; Michel, T.; Demirci, U. B.; Rouquette, J.; di Renzo, F.; et al., Anomalous Volume Changes in the Siliceous Zeolite Theta-1 TON Due to Hydrogen Insertion under High-Pressure, High-Temperature Conditions. *J. Phys. Chem. Lett.* **2021**, *12*, 5059-5063.

26. Alabarse, F. G.; Polisi, M.; Fabbiani, M.; Quartieri, S.; Arletti, R.; Joseph, B.; Capitani, F.; Contreras, S.; Konczewicz, L.; Rouquette, J., et al., High-Pressure Synthesis and Gas-Sensing Tests of 1-D Polymer/Aluminophosphate Nanocomposites. *ACS Appl. Mater. Interfaces* **2021**, *13*, 27237-27244.

27. Lapierre, R. B.; Rohrman, A. C.; Schlenker, J. L.; Wood, J. D.; Rubin, M. K.; Rohrbaugh, W. J., The Framework Topology of ZSM-12 - a High-Silica Zeolite. *Zeolites* **1985**, *5*, 346-348.

28. Fyfe, C. A.; Gies, H.; Kokotailo, G. T.; Marler, B.; Cox, D. E., Crystal-Structure of Silica-Zsm-12 by the Combined Use of High-Resolution Solid-State Mas Nmr-Spectroscopy and Synchrotron X-Ray-Powder Diffraction. *J. Phys. Chem.* **1990**, *94*, 3718-3721.

29. Kasunic, M.; Legisa, J.; Meden, A.; Logar, N. Z.; Beale, A. M.; Golobic, A., Crystal Structure of Pure-Silica ZSM-12 with Tetraethylammonium Cations from X-Ray Powder Diffraction Data. *Micropor. Mesopor. Mat.* **2009**, *122*, 255-263.

30. Prescher, C.; Prakapenka, V. B., Dioptas: A Program for Reduction of Two-Dimensional X-Ray Diffraction Data and Data Exploration. *High Pressure Res.* **2015**, *35*, 223-230.

31. Mao, H. K.; Xu, J.; Bell, P. M., Calibration of the Ruby Pressure Gauge to 800 Kbar under Quasi-Hydrostatic Conditions. *J. Geophys. Res.* **1986**, *91*, 4673-4676.

32. Murata, K.; Yokogawa, K.; Yoshino, H.; Klotz, S.; Munsch, P.; Irizawa, A.; Nishiyama, M.; Iizuka, K.; Nanba, T.; Okada, T, et al., Pressure Transmitting Medium Daphne 7474 Solidifying at 3.7 GPa at Room Temperature. *Rev. Sci. Instrum.* **2008**, *79*, 085101.

33. Rodriguez-Carvajal, J., Magnetic Structure Determination from Powder Diffraction Using the Program Fullprof. *Appl. Crystallogr.* **2001**, 30-36.

34. Momma, K.; Izumi, F., Vesta 3 for Three-Dimensional Visualization of Crystal, Volumetric and Morphology Data. *J. Appl. Crystallogr.* **2011**, *44*, 1272-1276.

35. Gonzalez-Platas, J.; Alvaro, M.; Nestola, F.; Angel, R., EosFit7-Gui: A New Graphical User Interface for Equation of State Calculations, Analyses and Teaching. *J. Appl. Crystallogr.* **2016**, *49*, 1377-1382.

36. SanchezPortal, D.; Ordejon, P.; Artacho, E.; Soler, J. M., Density-Functional Method for Very Large Systems with LCAO Basis Sets. *Int. J. Quantum Chem.* **1997**, *65*, 453-461.

37. Perdew, J. P.; Burke, K.; Ernzerhof, M., Generalized Gradient Approximation Made Simple. *Phys. Rev. Lett.* **1996**, *77*, 3865-3868.

38. Grimme, S., Semiempirical GGA-Type Density Functional Constructed with a Long-Range Dispersion Correction. *J. Comput. Chem.* **2006**, *27*, 1787-1799.

39. Birch, F., Equation of State and Thermodynamic Parameters of NaCl to 300-Kbar in the High-Temperature Domain. *J. Geophys. Res.-Solid.* **1986**, *91*, 4949-4954.

40. Im, J.; Yim, N.; Kim, J.; Vogt, T.; Lee, Y., High-Pressure Chemistry of a Zeolitic Imidazolate Framework Compound in the Presence of Different Fluids. *J. Am. Chem. Soc.* **2016**, *138*, 11477-11480.

41. Hobday, C. L.; Marshall, R. J.; Murphie, C. F.; Sotelo, J.; Richards, T.; Allan, D. R.; Duren, T.; Coudert, F. X.; Forgan, R. S.; Morrison, C. A., et al., A Computational and Experimental Approach Linking Disorder, High-Pressure Behavior, and Mechanical Properties in UiO Frameworks. *Angew. Chem. Int. Ed.* **2016**, *55*, 2401-2405.

42. Navarro-Sanchez, J.; Mullor-Ruiz, I.; Popescu, C.; Santamaria-Perez, D.; Segura, A.; Errandonea, D.; Gonzalez-Platas, J.; Marti-Gastaldo, C., Peptide Metal-Organic Frameworks under Pressure: Flexible Linkers for Cooperative Compression. *Dalton Trans.* **2018**, *47*, 10654-10659.

43. Ori, S.; Quartieri, S.; Vezzalini, G.; Dmitriev, V., Pressure-Induced Structural Deformation and Elastic Behavior of Wairakite. *Am. Mineral.* **2008**, *93*, 53-62.

44. Gatta, G. D.; Rotiroti, N.; Ballaran, T. B.; Pavese, A., Leucite at High Pressure: Elastic Behavior, Phase Stability, and Petrological Implications. *Am. Mineral.* **2008**, *93*, 1588-1596.

45. Collings, I. E.; Cairns, A. B.; Thompson, A. L.; Parker, J. E.; Tang, C. C.; Tucker, M. G.; Catafesta, J.; Levelut, C.; Haines, J.; Dmitriev, V., et al., Homologous Critical Behavior in the Molecular Frameworks $Zn(Cn)_2$ and $Cd(Imidazolate)_2$. *J. Am. Chem. Soc.* **2013**, *135*, 7610-7620.

46. Errandonea, D.; Boehler, R.; Japel, S.; Mezouar, M.; Benedetti, L. R., Structural Transformation of Compressed Solid Ar: An X-Ray Diffraction Study to 114 GPa. *Phys. Rev. B* **2006**, *73*, 092106.

TOC Graphic